HHS Public Access

Author manuscript

ACS Chem Biol. Author manuscript; available in PMC 2024 May 19.

Published in final edited form as:

ACS Chem Biol. 2023 May 19; 18(5): 1124–1135. doi:10.1021/acschembio.2c00919.

Benzothiazole Substitution Analogs of Rhodacyanine Hsp70 Inhibitors Modulate Tau Accumulation

Shannon E. Hill[1,2], **David Beaulieu-Abdelahad**[1,2], **Andrea Lemus**[3], **Jack M. Webster**[1,2], **Santiago Rodriguez Ospina**[1,2], **April L. Darling**[1,2], **Mackenzie D. Martin**[1,2], **Shreya Patel**[3], **Liznair Bridenstine**[3], **Ronald Swonger**[3], **Steven Paul**[1,2], **Roy Blackburn**[1,2], **Laurent Calcul**[3], **Chad A. Dickey**[1,2,5,#], **James W. Leahy**[1,3,4], **Laura J. Blair**[1,2,5,*]

[1]Department of Molecular Medicine, Morsani College of Medicine, University of South Florida, Tampa, FL 33612, USA

[2]USF Health Byrd Alzheimer's Institute, University of South Florida, Tampa, FL 33612, USA

[3]Department of Chemistry, University of South Florida, 4202 East Fowler Avenue, CHE 205, Tampa, Florida 33620, USA

[4]Center for Drug Discovery and Innovation, University of South Florida, 3720 Spectrum Boulevard, Suite 303, Tampa, Florida 33612, USA

[5]Research Service, James A Haley Veterans Hospital, 13000 Bruce B Downs Blvd, Tampa, FL 33612, USA

Abstract

The accumulation and aggregation of the microtubule-associated protein tau (tau) into intracellular neuronal tangles is a hallmark of a range of progressive neurodegenerative tauopathies; including Alzheimer's disease (AD), frontotemporal dementia, Pick's disease, and progressive supranuclear palsy. The aberrant phosphorylation of tau is associated with tau aggregates in AD. Members of the heat shock protein 70 kDa (Hsp70) family of chaperones bind directly to tau and modulate tau clearance and aggregation. Small molecules that inhibit the Hsp70 family of chaperones have been shown to reduce the accumulation of tau, including phosphorylated tau. Here, eight analogs of the rhodacyanine inhibitor, JG-98, were synthesized and evaluated. Like JG-98, many of the compounds inhibited ATPase activity of the cytosolic heat shock cognate 70 protein (Hsc70) and reduced total, aggregated, and phosphorylated tau accumulation in cultured cells. Three compounds, representing divergent clogP values, were evaluated for *in vivo* blood brain barrier penetration and tau reduction in an *ex vivo* brain slice model. AL69, the compound with the lowest clogP and the lowest membrane retention in a parallel artificial membrane permeability

[*]**Corresponding Author:** Laura J Blair – laurablair@usf.edu.

[#]Deceased

Author Contributions

C.A.D., J.W.L., and L.J.B. conceived the study. S.E.H., A.L., L.C., J.W.L., and L.J.B. designed experiments. S.E.H., D.B.A, A.L., A.L.D., S.R.O., M.D.M., S.P., L.B., R.S., S.P. R.B., and L.C. performed experiments. S.E.H., D.B.A, A.L., J.M.W., S.R.O., A.L.D., L.C., and L.J.B. analyzed the data. S.E.H., A.L., J.M.W., J.W.L., and L.J.B. wrote the paper. All authors reviewed and contributed to the manuscript. All authors have given approval to the final version of the manuscript, with the exception of Dr. Chad Dickey, who is deceased.

Supporting Information.

The Supporting Information is available free of charge via the Internet at http://pubs.acs.org

assay (PAMPA), reduced phosphorylated tau accumulation. Our results suggest that benzothiazole substitutions of JG-98 that increase hydrophilicity may increase the efficacy of these Hsp70 inhibitors to reduce phosphorylated tau.

Graphical Abstract

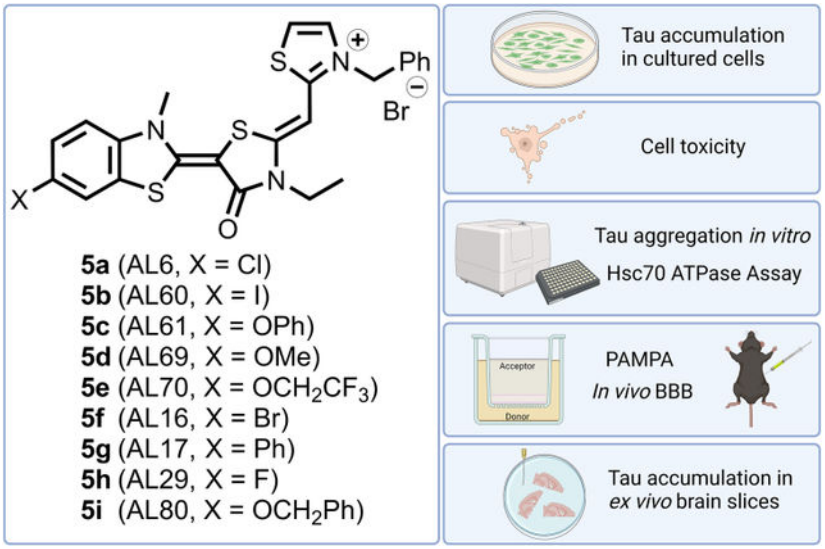

Keywords

Tau; MAPT; Hsp70 inhibitors; JG-98; rhodacyanine

The accumulation of the microtubule associated protein tau into misfolded oligomers, fibrils, paired helical filaments, and neurofibrillary tangles is a common feature of many neurodegenerative diseases, termed tauopathies[1–5]; these include Alzheimer's disease (AD), frontotemporal dementia (FTD), Pick's disease (PiD), and progressive supranuclear palsy (PSP). Mutations in the gene encoding tau, *MAPT*, are causative for FTD. P301L tau is one of the most common mutations[6], which shows a high propensity to aggregate[7]. The hyperphosphorylation of tau is also associated with its aggregation, particularly in AD[8, 9]. Currently, there are no effective treatments for these diseases. Potential therapeutic strategies include enhancing the clearance of tau or tau aggregates, facilitating the refolding of misfolded tau, or sequestering toxic forms of tau[10]. Modulating the heat shock protein 70kDa family (HSPA) of ATP-dependent molecular chaperones have demonstrated neuroprotection in neurodegenerative tauopathy models[11–14].

Molecular chaperones, including HSPAs, bind to and promote refolding, facilitate degradation, or regulate sequestration of client proteins in order to maintain a normal cellular homeostasis[15, 16]. There are 13 genes in the human HSPA family that encode both constitutively active members like the cytosolic heat shock cognate 70 (Hsc70/HSPA8) and stress-inducible members like heat shock protein 70 (Hsp70, Hsp72/HSPA1A)[17]. The role of HSPAs in the clearance of tau differs depending on the chaperone ATPase activity as well as the assortment of additional chaperones, co-chaperones and binding partners

recruited to multi-subunit chaperone complexes. Hsc70 has been shown to bind directly to phosphorylated tau in the AD brain[18] and interacts with tau in human iPSC-derived neurons[19]. While both major cytosolic forms bind to tau, Hsp70 works to both inhibit aggregation and sequester tau oligomers and fibrils[14], promoting the clearance of tau, while Hsc70 slows degradation, preserving tau protein[20, 21]. In addition, dominant negative Hsc70 mutants that lack ATPase activity potently enhance proteasomal degradation of tau[22], which supports HSPA inhibition as a potential mechanism to accentuate tau degradation. Small molecule inhibitors that bind the nucleotide-binding domain (NBD), either competitively in the ATP binding site or non-competitively at an allosteric site, prevent ATP hydrolysis and lock Hsp70 in the "open" or "closed" state[20, 23–25], thereby promoting the proteasomal degradation of tau[26]. These small molecule inhibitors, which include derivatives of the rhodacyanine scaffold, have been studied broadly to inhibit HSPA function for cancer therapeutics and to prevent the accumulation of tau[27–29].

The first identified rhodacyanine to bind to an allosteric site on Hsp70 and prevent cellular tau accumulation was MKT-077[24]. Although MKT-077 is a promising lead, the low potency, weak selectivity, mitochondrial localization, and poor membrane permeability of MKT-077 has driven structure-based efforts to develop improved molecules. The first derivative of MKT-077, YM-01[30, 31] enhanced the potency to prevent tau accumulation in HeLaC3 cells, increased cytosolic localization, and reduced pathogenic tau in *ex vivo* brain slices from transgenic rTg4510 mice, however YM-01 lacked detectable blood-brain permeability[32]. In an effort to improve permeability, a second neutral derivative, YM-08 was developed in which the cationic pyridinium was replaced with a neutral pyridine. In *ex vivo* rTg4510 brain slices, YM-08 reduced phospho-tau but no reduction in total tau was reported, consistent with the reduced potency of YM-08 to prevent tau accumulation in HeLaC3 cells when compared to MKT-077 and YM-01[32]. As predicted, the neutral derivative, YM-08, resulted in blood brain permeability, however YM-08 was metabolically unstable with a half-life less than three minutes[32].

In an effort to remove metabolic liabilities, an MKT-077 analog, JG-98, which replaced the 2-pyridyl with 2-thizolyl combined with a 5-Cl substitution, had substantially increased half-life ($t_{1/2}$ = 37 minutes)[33], greater potency to prevent cellular tau accumulation than YM-01 and reduced total tau in organotypic brain slices from rTg4510 mice[22]. JG-98 exhibits high specificity to the HSPA family, compared to other HSPA inhibitors, and does not elicit a heat shock response[34]. Due to the interfering spectral properties of cationic rhodacyanine molecules, neutral analogs of JG-98, such as JG-48[13] and JG2–38[35], have been synthesized to investigate mechanisms of action, however the neutrality is predicted to be a metabolic liability, thereby preventing *in vivo* utility.

Using the JG-98 rhodacyanine scaffold and focusing on benzothiazole substitutions to improve blood-brain barrier (BBB) penetrance, we have developed and tested a series of HSPA inhibitor JG-98 analogs. Analogs discussed here include aryl halide substitution of iodine, bromine, or fluorine for chlorine; as well as a phenyl substitution and ether analogs at the same position. Our results demonstrate that most of these compounds inhibit Hsc70 ATPase activity and alter total, phospho-, and insoluble tau accumulation in cultured cells. Tau potency was also measured in *ex vivo* slices from the brains of tau transgenic mice for

three compounds with varying membrane retention, as determined by a blood-brain barrier parallel artificial membrane permeability assay (PAMPA). Overall, this work suggests that modifications to the JG-98 scaffold that increase hydrophilicity may be more potent towards regulating tau in brain tissues.

RESULTS

Chemical synthesis of JG-98 analogs.

As the structure-activity relationship of the HSPA rhodacyanine scaffold matured from MKT-077 through YM-01 and YM-08 to JG-98 (Figure 1A), it became clear that the issue of BBB penetrance combined with potency had not been resolved and that neutral analogs, such as YM-08 and JG-48, were significant metabolic liabilities[36]. We, therefore, focused on the JG-98 scaffold containing the constitutively charged ethyl thiazole ring and developed benzothiazole substitutions (Figure 1B) to test for potency against tau accumulation and membrane permeability. The rationale for benzothiazole substitution is that the benzothiazole of JG-98 is predicted to bind at an allosteric site of HSPA that is oriented toward the nucleotide binding site (Figure S1). A prediction agrees with previously published models and NMR chemical shift perturbations[13, 33, 36, 37]. Small substitutions such as halogenation are anticipated to maintain activity but may show improved membrane permeability. We therefore synthesized JG-98 analogs as shown in Figure 1B, whose viability was demonstrated by the synthesis of AL6 (**5a**) and isolation of the product as the bromide salt. AL6 was shown to have identical tau lowering effects to JG-98 (Figure S2). The requisite orthochloroanilines were either obtained commercially or prepared via Ullman reaction from **1** with the appropriate alcohol to give **2**. AL17 (**5g**) was synthesized directly from AL16 (**5f**) with phenylboronic acid under standard Suzuki conditions.

Tau P301L protein levels decrease in cultured cells treated with rhodacyanine analogs.

To determine if our compounds could lower tau levels in mammalian cells, as shown for prior rhodacyanine inhibitors[22, 28], inducible tau P301L-expressing HEK293T cells were treated with 0.5% DMSO (vehicle) or increasing concentrations of the indicated rhodacyanine compounds for 24 hours. Cell lysates were evaluated by Western blot with antibodies immunoreactive to phosphorylated and total tau protein (Figure 2). AL6 reduced total tau levels, regardless of the densitometry analysis being around the ~50kda tau band or the full lane, and also reduced phosphorylated tau levels, consistent with Figure S2. When analyzing the ~50kDa tau band alone, all AL-series compounds except AL61, AL70, and AL17 reduced total tau levels, with AL61 trending toward significance (Figure 2B). When performing the full lane analysis, AL69, AL16, AL29 and AL80 significantly reduced phospho- and total tau levels, similar to AL6 (Figure 2C). When comparing compounds at the same concentration, none of the compounds had a greater reduction of total tau or phosphorylated tau levels relative to our benchmark compound AL6 when evaluated by one way ANOVA using Dunnett’s post-hoc comparison.

Rhodacyanine analogs do not cause toxicity, except for AL61.

Toxicity of the eight rhodacyanine analogs were tested in SH-SY5Y human neuroblastoma cells (Figure 3). With the exception of AL61 at 10 μM, these compounds did not result in

measurable toxicity compared to DMSO vehicle control. AL61, the phenyl ether-containing analog, significantly increased the levels of extracellular LDH, suggesting toxicity in this cell line at 10 μM. This compound may be disfavored unless it exhibits desirable traits (like BBB permeability) that distinguish it from other compounds.

Most rhodacyanine analogs inhibit Hsc70 ATPase activity.

Traditionally, HSPA ATPase activity has been determined using malachite green to quantify the production of free orthophosphate by absorbance at 600 nm, however the charged pyridinium of molecules like JG-98 and the AL-series compounds have fluorescent overlap with malachite green making them incompatible with this assay[13, 29, 38]. Therefore, a commercially available luciferase-based assay, ADP-Glo™ kinase assay, was used to assess AL-series compatibility. The addition of AL6 at 30 μM had no effect, slope or signal, on the ADP standard curve consisting of 0 to 50 μM ADP in the presence of 1% DMSO (vehicle) (Figure 4A). The ATPase activity of Hsc70 in the presence of DnaJA2 and 1% DMSO (vehicle) produced a luminescence signal within the ADP standard curve, consistent with previous Hsc70 ATP turnover rates[13, 38, 39]. Next, Hsc70 ATPase activity in the presence of increasing concentrations (3, 10, and 30 μM) of each compound, showed most compounds inhibit ATPase activity similar to AL6 (Figure 4B). The weak inhibition of Hsc70 ATPase activity by the AL-series compounds is consistent with other non-competitive ATP inhibitors of the JG-98 scaffold. For instance, the neutral analog, JG-48, at 50 μM, previously showed only 31–60% inhibition of Hsc70 ATPase activity while still reducing cellular tau at a much lower dose of 10 μM[13]. Two compounds, AL70 with a trifluorethyl ether substitution and AL17 with a phenyl substitution, had no effect on Hsc70 ATPase activity, regardless of concentration, suggesting large or rigid substitutions may prevent Hsc70 binding. In agreement with the lack of ATPase inhibition, AL17 and AL70 were also the only two compounds to have no effect on cellular tau levels in iHekP301L cells by Western blot analysis of the ~50 kDa tau band, as shown in Figure 2. Overall, reduction of Hsc70 ATPase activity by AL-series compounds corresponded with reduced cellular tau.

Rhodacyanine derivatives do not directly modulate heparin-induced tau P301L aggregation.

Prior data suggested that rhodacyanines, in addition to HSPA-dependent activity, may directly inhibit tau aggregation[28]. To determine if our rhodacyanine analogs also had this effect, heparin-induced *in vitro* tau P301L aggregation assays were performed in the presence of DMSO (vehicle) or the first five rhodacyanine derivatives in the AL-series, including AL6. Only the DMSO control demonstrated the expected increase in ThT fluorescence activity over 5 days, indicative of tau fibril formation. Each of the compounds tested in the presence of tau prevented the increase in Thioflavin T (ThT) signal, this effect was maintained over 5 days, as shown in Figure 5A. It is important to note that all compounds significantly reduced intrinsic ThT fluorescence by almost 40% (ThT intensity = ~113 RFU in the presence of each compound compared to ~181 RFU for DMSO alone) (Figure 5B). This suggests that these compounds may have spectroscopic properties that interfere with ThT fluorescence, the compounds alone interact with ThT directly, or the compounds alter ThT affinity for tau protein. To determine whether tau aggregation was prevented, samples containing DMSO (vehicle) or the first two rhodacyanine derivatives in

the AL-series, AL6 and AL60, were evaluated by transmission electron microscopy (TEM) at the endpoint of the ThT assay (Figure 5C). TEM images showed robust fibrilization of tau protein in the DMSO control as well as in the presence of AL6 and AL60. These results indicate that the lack of ThT fluorescence signal does not represent inhibition of tau fibril formation in the presence of these compounds, since TEM images clearly show tau fibrils following AL6 and AL60 incubation. The remaining rhodacyanine analogs were not further evaluated, by ThT fluorescence or TEM imaging, given the benchmark compound, AL6, did not directly inhibit tau aggregation.

All rhodacyanine compounds lack BBB permeability but have variable membrane retention levels.

A parallel artificial membrane permeability assay (PAMPA) was used to determine permeability, using the Pion BBB-1 phospholipid mixture (Figure 6A). AL6 and all eight of the rhodacyanine analogs tested showed no observable permeability into the acceptor sink buffer after 24 hours. Membrane retention was calculated by measuring the initial compound concentration and subtracting the concentration in the acceptor and donor sink after 24 hours. Retention of the compounds in the membrane was observed for all AL-series compounds and correlated well with the predicted logP values (clogP), as shown in Figure 6B. Membrane retention ranged from 31–95% with lower membrane retention due to higher compound concentration remaining in the donor sink. The methyl ether analog (AL69) exhibited the lowest membrane retention, while the benzyl ether analog (AL80) demonstrated the highest membrane retention. The benchmark compound (AL6) demonstrated a mid-range membrane retention. These results showed none of the AL-series compounds crossed the membrane by passive diffusion but suggests increased hydrophilicity prevents compounds from being trapped in the membrane.

Although PAMPA can be utilized as a predictor of BBB permeability, there are limitations to PAMPA that do not entirely represent the BBB, such as a lack of active transporters and cellular composition[40, 41]. To validate that the AL-series compounds are BBB impermeable as predicted by PAMPA, mice were treated with AL6, AL69, or AL80 by intraperitoneal (i.p.) injection, after 1 hour brain tissue and blood plasma harvested for measurement of compound concentration by LC-MS. As expected, AL6, AL69, and AL80 were not detected at appreciable levels in the brain with brain/plasma (B/P) ratios less than 0.015 (Figure S3).

Insoluble tau P301L protein levels decrease in cultured cells treated with rhodacyanine analogs.

Prior work has shown that HSPA inhibitors promote degradation of tau, but whether HSPA inhibitors alter soluble and insoluble states of cellular tau has been weakly explored[26]. In order to determine whether rhodacyanines alter soluble and insoluble tau levels, we first had to establish that insoluble tau accumulation could reach an appreciable level in iHekP301L cells with only 24 hours tetracycline induction, given our prior work involved 3–5 days tetracycline induction[42, 43]. To accomplish this, iHekP301L cells were plated with tetracycline for 24 hours followed by treatment with 0.5% DMSO (vehicle) or AL6 at 10 μM for 24 hours. Cell lysis was performed using Triton X-100, a mild non-ionic detergent, and tau protein was fractionated into total, Triton-soluble and Triton-insoluble protein for

evaluation by Western blot. For vehicle-treated iHekP301L cells, insoluble tau was clearly visible by Western blot and AL6 treatment significantly reduced total, soluble, and insoluble tau (Figure S4).

AL69 and AL80 were next selected to represent different membrane retention profiles with similar cellular tau reduction attributes as AL6, to determine if AL69 and AL80 also reduce the accumulation of soluble and insoluble tau. Both AL69 and AL80, significantly reduced total, soluble and insoluble tau (Figure 7). For all three compounds, the percent reduction of insoluble tau was greater than the percent reduction of total or soluble tau. These results, when combined with the ATPase activity assay and heparin-induced tau aggregation assay, suggest that inhibiting HSPA ATPase activity with rhodacyanines prevents the accumulation of insoluble cellular tau, through HSPA inhibition.

Low membrane retention of rhodacyanine compounds corresponds with reduced phospho-tau accumulation in brain tissue.

AL6, AL69, and AL80 were again selected to represent different membrane retention profiles and evaluated in an acute *ex vivo* brain slice assay to determine effects on tau protein levels. rTg4510 mice were selected since they express P301L tau on the CamKIIα promoter[44]. This results in progressive tau accumulation throughout the forebrain including phosphorylated tau species by 3 months of age and aggregated tau by 6-months of age, which has been well characterized[45]. We used *ex vivo* slices pooled from three 7-month-old rTg4510 mice for each treatment. AL69 dose dependently reduced PHF1 phospho-tau levels compared to DMSO control, which reached significance at 10 μM (Figure 8). There was also a significant reduction in PHF1 phospho-tau compared to AL6 and AL80 at this concentration. AL6 showed a slight trend toward increasing PHF1 phospho-tau at 10 μM that did not reach significance, which was surprising, since this was counter to the iHekP301L cellular data, where PHF1 phospho-tau was reduced upon AL6 treatment. Given AL6, AL69, and AL80 had similar potency at reducing tau accumulation in iHekP301L cells, as shown in Figure 2, the *ex vivo* brain slice results suggest the increased efficacy of AL69 towards reducing phospho-tau may be driven by increased hydrophilicity.

DISCUSSION

Many classes of HSPA inhibitors have been shown to affect tau accumulation. The phenothiazine class, which includes methylene blue (MB)[46] and the Azure series of derivatives[47], appears to have multiple molecular mechanisms that affect tau. MB inhibits HSPA ATPase activity resulting in reduced tau levels[28, 48], but also has been suggested to reduce tau fibrilization directly[46, 49]. The mechanism of action for these phenothiazine compounds appears to be through oxidation of cysteine residues, an effect not selective for tau and HSPA[49]. The clinical failure of these compounds may be linked to this non-specific mechanism and/or to the inhibition of tau fibrilization favoring the accumulation of smaller toxic oligomers[46]. From the flavanol class, myricetin inhibited tau aggregation *in vitro* and reduced tau levels in a HeLa cell model, suggesting effects on tau directly as well as through HSPA inhibition[26, 50].

The rhodacyanine class of inhibitors, MKT-077[24], YM-08[32], and JG-98[13, 22, 28], bind to an allosteric site within the nucleotide-binding domain of HSPA, adjacent to the ATP/ADP docking site, some of which are reported to inhibit tau aggregation and/or reduce cellular tau levels. Here, we evaluated additional rhodacyanine scaffold analogs, based on a bromide salt form of the JG-98 scaffold (AL6), which can be easily generated via the bromide salt of **7**. Using the bromide salt did not affect the anti-tau activity but improved the synthetic yield. The substitution pattern about the benzothiazole group was designed to target the narrow pocket previously proposed to point toward the nucleotide binding site on HSPA. We selected ether linkages in part to enable adequate flexibility to adopt an optimal orientation in this pocket.

Five of the AL-series compounds examined using an *in vitro* heparin-induced aggregation assay showed inhibition of ThT fluorescence when included with tau P301L. Yet inhibition of tau fibril formation was not evident via TEM imaging. Other compounds have been reported to interfere with ThT fluorescence aggregation assays[51–53]; therefore, it is common practice to not rely on ThT results alone to monitor aggregation. Here, we conclude that ThT assays are not compatible with this class of compounds at ~10 μM, most likely due to fluorescent properties of the charged pyridinium group on the JG-98 scaffold. Therefore, we did not evaluate the remaining AL compounds with a ThT assay. A recent study shows that replacement of this charged pyridinium with a neutral pyridinium can significantly reduce intrinsic fluorescence while maintaining HSPA-related activity[29], providing a new scaffold that may be suitable for fluorescence-based biochemical and cellular assays. Therefore, while certain tau reducing compounds may have mechanisms that include both HSPA inhibition and direct interactions with tau, here we conclude that rhodacyanine compounds show little evidence for direct inhibition of tau aggregation *in vitro*.

All rhodacyanine analogs in the AL-series modulated tau levels in mammalian cells, with AL17 (X = Ph) and AL70 (X = OCH2CF3) showing the least tau reducing activity, an effect which corresponded with the lack of HSPA ATPase inhibition for AL17 and AL70. While we hypothesized that the fluorinated analog would provide improved pharmacokinetics by limiting the metabolic liability of the ether appendage, none of the rhodacyanine analogs tested allowed for membrane permeability. A comparison of compounds with high (AL80), medium (AL6), and low (AL69) membrane retention profiles in tau P301L expressing *ex vivo* brain slices, suggests that efforts to decrease membrane retention characteristics result in improved effects on reducing phospho-tau accumulation. The nature of these substituents (specifically, X = OCH_2Ph, Cl and OMe, respectively) suggests that flexible substitution is preferred for achieving this goal. Overall, our data suggest membrane retention appears to be a characteristic that is tunable with benzothiazole substitutions, which may enable the synthesis of BBB-penetrant derivatives that maintain or improve potency towards the modulation of tau.

METHODS

Reagents and Antibodies.

JG-98 was generously provided by J. Gestwicki (University of California, San Francisco, CA). All compounds were solubilized in DMSO (Sigma-Aldrich, St. Louis, MO). Tau5

was a gift from Nicholas Kanaan at Michigan State University (originally created by Lester Binder at Northwestern University), anti-PHF1 was a gift from Peter Davies from Albert Einstein University, anti-phospho-tau threonine 231 (pT231) was purchased from AnaSpec (Freemont, CA), anti-tau (H-150) was purchased from Santa Cruz Biotech (Dallas, Tx) and anti-GAPDH and anti-β Actin was purchased from ProteinTech (Rosemont, IL). HRP-tagged secondary antibodies were purchased from Southern Biotech (Birmingham, AL). All primary and secondary antibodies were diluted in 7% nonfat dry milk (Research Products International, Mt. Prospect, IL) in 1X Tris-buffered saline (TBS).

Chemical Synthesis.

The full experimental details for the synthesis of each of the new compounds is described in Figure 1. Each synthesized compound was determined to be >95% pure by HPLC analysis, and the structures confirmed by NMR and high-resolution mass spectrometry. Detailed analytical data for each compound is provided in the Supplemental Procedures.

Protein Expression and Purification.

E. coli BL21 cells were transformed with 4R0N tau P301L inserted into a pET28a vector with an engineered 6x histidine tag and TEV protease site. For 4R0N tau P301L production, cells were grown at 37°C in LB media containing 100 μg/mL kanamycin. When the OD600 reached 0.8 the cells were induced with 1 mM of IPTG (Gold Biotechnology, Olivette, MO) for 3 hours. Centrifugation at 5,000 × *g* for 20 min was used to pellet the cells, which were then resuspended with nickel chromatography running buffer (20 mM Tris-HCl pH 8.0, 500 mM NaCl, 10 mM Imidazole) containing protease inhibitors. Then the cells were lysed using a freeze-thaw cycle followed by sonication. The lysed cells were centrifuged at 50,000 × *g* for 30 minutes at 4°C. The supernatant was purified using affinity purification with a standard gravity column packed with HisPur™ Ni-NTA Resin (Fisher Scientific, Hampton, NH). Eluted fractions were treated with TEV protease for 4 hours at room temperature then dialyzed in nickel chromatography running buffer overnight. A second nickel purification column was run, and cleaved tau protein was collected in the flow through, the relative amount of uncleaved tau in the eluted fractions was also assessed by SDS-PAGE followed by Coomassie staining. Size exclusion chromatography was used to further purify tau protein with a HiLoad 16/600 Superdex 200 pg column. Protein fractions were pooled and concentrated to 2 mg/mL. The concentrated protein samples were then aliquoted, flash frozen with liquid nitrogen, and stored at −80°C until use. Hsc70 and DnaJA2 were grown similarly, except Hsc70 and DnaJA2 were treated with TEV for 5 hours to ensure full His cleavage before further purification.

Cell Culture.

Tetracycline-regulatable 0N4R tau P301L stably expressing HEK293T cells (iHekP301L)[20, 42, 43] were maintained in DMEM (Corning, Corning, NY) plus 10% FBS (VWR, Radnor, PA), and 1% penicillin/streptomycin (Invitrogen, Waltham, MA). Cells were induced with tetracycline hydrochloride (Sigma-Aldrich, St. Louis, MO) for 24 hours, then treated with compounds at 1 μM, 3 μM, and 10 μM respectively for 24 hours. Cells were harvested in RIPA buffer (150 mM sodium chloride, 1.0% Triton X-100, 0.5% sodium deoxycholate, 0.1% SDS, 50 mM Tris [pH 8]) containing protease and phosphatase inhibitor

cocktails (complete RIPA). Human neuroblastoma cells (SH-SY5Y, ATCC, Manassas, VA) were maintained in Advanced DMEM/F12 (Life Technologies, Carlsbad, CA) with 10% FBS and 1% penicillin/streptomycin. Cells were plated onto 12-well plates at 80% confluency then treated with compounds at 1 μM, 3 μM, and 10 μM, respectively, for 24 hours prior to removal of media for LDH cytotoxicity assay.

For Triton-soluble and Triton-insoluble fractionation in 10 cm dishes, iHekP301L cells were detached by pipetting, washed with 8mL of PBS buffer, and lysed in 1 mL of Triton X-100 lysis buffer consisting of 50 mM Tris base pH 8.0, 150 mM NaCl, 5 mM EDTA, and 1% Triton X-100 supplemented with protease and phosphatase inhibitor cocktails. After 10 min on ice, lysed cells were centrifuged at 3,000 × *g* for 10 minutes to remove cell debris and 100 μL of the supernatant was removed for further analysis. The remaining supernatant was then centrifuged at 21,000 × *g* for 30 min and the high-speed supernatant isolated as the Triton-soluble fraction. The high-speed pellet was then resuspended with 1 mL of Triton X-100 lysis buffer to wash the pellet and re-pelleted by centrifugation at 21,000 × *g* for 30 min. All centrifugation steps were performed at 4°C. The final pellet or Triton-insoluble fraction was resuspended in a buffer containing 8 M urea, 50 mM Tris base pH 8.0, 2% SDS, 10 mM EDTA, and sonicated at room temperature for 3 pulses at 25% amplitude for 5 s on/10 s off. Total protein concentration from the initial supernatant was measured by bicinchonic acid assay (BCA; ThermoFisher Scientific, Waltham, MA) and used to load equal amounts of soluble and insoluble protein.

LDH Cytotoxicity Assay.

Media was collected from treated SH-SY5Y cells and used to perform a Lactate Dehydrogenase (LDH) cytotoxicity assay using the Pierce LDH cytotoxicity assay kit (ThermoFisher Scientific, Waltham, MA) as recommended by the manufacturer. Values are presented as the percent of LDH release compared to a control well of lysed cells representing 100% toxicity. Statistical analysis compares samples to a DMSO vehicle control treatment.

Hsc70 ATPase Activity Assay.

The ADP-Glo™ kinase assay (Promega, V6930) was used to measure ATPase activity of recombinant Hsc70 in the presence of increasing concentrations (3, 10, and 30 μM) of each AL-series compound or 1% DMSO (vehicle). Prior to setting up the ATPase reaction, recombinant Hsc70 and DnaJA2 proteins were dialyzed overnight at 4°C in the ATPase assay buffer composed of 40 mM Tris pH 7.5 and 20 mM $MgCl_2$. Following dialysis, any protein precipitation was removed by spinning the samples at 2,300 g at 4°C for 10 minutes and collecting the supernatant. ATPase reactions were performed at 37°C for 3 hours in a volume of 100 μL consisting of 1 μM Hsc70, 1 μM DnaJA2, 1mM ATP, and the appropriate AL-series compound or 1% DMSO (vehicle). Hsc70, DnaJA2, and compound were pre-incubated for 30 minutes at room temperature prior to the addition of ATP. At the termination of each reaction, 10 μL reaction volume was added in triplicate to a white, opaque 96 well half-area microplate (Corning, CLS3693), followed by 10 μL ADP-Glo™ reagent, and 20 μL detection reagent with the appropriate incubation times as described in

the manufacturers' instructions. Luminescence signal was measured using a Biotek Synergy H1 and confirmed to be within the linear range of the ADP standard curve.

Thioflavin T Aggregation Kinetics Assay.

Recombinant human P301L tau was dialyzed into 100 mM sodium acetate buffer pH 7.4 overnight. Samples consisting of 20 μM P301L tau and 2x the indicated concentration of compound were incubated at room temperature for 1 hour prior to starting the assay. Using a master mix of 2x concentrated heparin (MP Biomedicals, Santa Anna, CA), Thioflavin T (Sigma-Aldrich, St. Louis, MO), and dithiothreitol (ThermoFisher Scientific, Waltham, MA), samples were diluted to a final concentration of 10 μM P301L tau, 2.5 μM heparin, 10 μM thioflavin T, the compounds at indicated concentrations or DMSO, and 2 mM dithiothreitol in 100 mM sodium acetate at pH 7.4. A total of 200 μL was added to each well of a low binding 96-well black sided clear bottom costar plate (Corning, Corning, NY). Each plate was incubated at 37 °C, and fluorescence intensity (440 excitation, 482 emission) was measured over a 5-day period using a BioTek (Winooski, VT) Synergy H1 microplate reader.

TEM.

Following ThT aggregation assays, 10 μL of each sample was adsorbed onto square mesh copper grids (CF300-Cu) for 45 seconds. Grids were washed twice with 10 μL of deionized water, and the excess water was removed. Samples were negatively stained with 2% uranyl acetate for 45 seconds and dried overnight in desiccant. Grids were viewed using a JEOL 1400 Digital Transmission Electron Microscope, and images were captured with a Gatan Orius wide-field camera. To prevent bias, grids were systematically scanned and at least 3 overview images at 8,000× magnification were acquired before imaging at the higher magnification, 60,000×, shown.

Western Blotting.

Following cell lysis, samples were cleared by centrifugation at 10,000 × *g* for 5 minutes and protein concentrations were normalized by BCA. Cell lysate samples were prepared with 2x Laemmli containing β-mercaptoethanol (βME) and denatured using 100 °C for 10 minutes. *Ex vivo* brain slice lysates were processed using the same methods. Samples were run on 5–20% gradient or Any kD TGX Precast gels (Bio-Rad, Hercules, CA) then transferred to PVDF membranes (Immunobilon, EMD Millipore, Burlington, MA). The membranes were then blocked with 7% nonfat dry milk diluted in 1x TBS for 1 hour prior to being probed overnight at 4°C against the primary antibody. The primary antibodies were then detected by species specific secondary antibodies and chemiluminescence was observed using an ECL Western blot detection reagent using an ImageQuant LAS 4000 (GE Healthcare, Chicago, IL). Immunoreactive signal was quantified with BioRad Image Lab software. Values shown represent mean intensities of the antibody used relative to GAPDH and normalized to the mean of the DMSO control condition.

Parallel artificial membrane permeability assay.

Compounds were evaluated by Pion, Inc. (Billerica, MA) for permeability using a Blood Brain Barrier-PAMPA assay. 10 mM stock solutions in DMSO were diluted to 100 μM in PRISMA buffer (pH 7.4). 150 μL of diluted compound was placed in a UV plate reader to obtain the reference spectrum for each compound. Six replicates of 200 μL of each diluted compound were used to fill the PAMPA donor plate, as well as DMSO controls. The precoated BBB lipid acceptor plate was filled with 200 μL BBB acceptor sink buffer. The PAMPA sandwich was placed together and incubated in dark at room temperature for 24 hours. Aliquots of the donor and acceptor plate were taken, and UV spectra were obtained to quantitate compounds. UV spectra were compared to the reference spectra for each compound.

In vivo blood brain barrier permeability.

All procedures involving animal subjects were performed in accordance with the guidelines set forth by the Institutional Animal Care and Use Committee (IACUC) at the University of South Florida. For assessment of blood brain barrier penetration, 10-weeks old C57BL/6J mice (Jackson Laboratory, stock #00064) were treated with AL6, AL69, or AL80 at 3 mg/kg by i.p. injection. The plasma and brain were collected 1 hour after injection. Plasma was obtained by collecting 200 μL whole blood in tubes containing 60 μL 0.5 M EDTA, pH 8 on ice, followed by centrifugation at 3000 × *g* for 10 min at 4 °C to isolate supernatant. Brain tissue homogenates were prepared by adding three volumes ice-cold PBS with 5% bovine serum albumin (BSA) and homogenizing for 3 min using an IKA T10 Basic S1 disperser at speed 5.5. Plasma (brain) samples of 75 μL (150 μL) were added to 150 μL methanol. Samples were allowed to rest on ice for 15 min and then centrifuged at 12,000 rpm and 4°C for 15 min. Clarified supernatants were transferred to vials and analyzed by tandem mass spectrometry. The LC-MS analysis was performed using an Agilent 1260 HPLC on a Kinetex PolarC18 column (4.6 × 100 mm, 2.6 μm; Phenomenex) at 40°C under ACNaq (+0.1% formic acid) gradient condition of 30–30% over 1 min, 30–95% over 6 min, 95% over 3 min, 95–30% over 0.5 min, 30–30% over 1.5 min with 1 min equilibration time at a flow rate of 0.5 mL/min. The HPLC was coupled with an Agilent triple quadruple mass spectrometer 6460 equipped with an electrospray ionization (ESI) source using the Agilent Jet Stream technology. The samples were injected at a volume of 1 μL and analyzed using positive mode with capillary voltage at 4000V, gas temperature at 300 °C, gas flow rate at 10 L/min, nebulizer pressure at 20 PSI, sheath heater at 350 °C, sheath gas glow at 7.5 L/min. Data acquisition were controlled by the Agilent Mass hunter acquisition software B05 and the MRM transitions were optimized at fragmentor voltage of 88 V and collision energy of 25 V for **5a** (AL6) m/z 498.0 → 407.0, **5d** (AL69) m/z 494.1 → 403.0 and **5i** (AL80) m/z 570.1 → 479.1.

Ex vivo brain slice assay.

Acute brain slices were prepared and processed, as previously described[31]. Seven-month-old rTg4510 mice were euthanized by rapid decapitation, and whole brains were rapidly removed and submerged in ice cold cutting solution (110 mM Sucrose, 60 mM NaCl, 3 mM KCl, 1.25 mM NaH_2PO_4, 28 mM $NaHCO_3$, 5 mM Glucose, 0.6 mM Ascorbate, 0.5

mM $CaCl_2$ (Dihydrate), and 7 mM $MgCl_2$ (Hexahydrate). Horizontal slices of 400 μm were generated with a vibratome (Thermo Microm HM650V). Once sectioned, tissue was placed in a room temperature solution for 10 minutes made of cutting solution (50%) and Artificial Cerebrospinal Fluid (50%; ACSF) – 125 mM NaCl, 2.5 mM KCl, 1.25 mM NaH_2PO_4, 25 mM $NaHCO_3$, 25 mM Glucose, 2 mM $CaCl_2$ (Dihydrate), and 1 mM $MgCl_2$ (Hexahydrate). Slices were then place in ACSF at 32°C for 15 minutes and then treated with AL compounds, AL6, AL69, AL80 at 10, 3.33, and 1.11 μM or DMSO control. Slices were harvested after 6 hours and lysed in mammalian protein extraction reagent (MPER; ThermoFisher Scientific, Waltham, MA) containing protease and phosphatase inhibitors. A Pellet Pestle was then used to disrupt tissue, which was allowed to incubate for 30 minutes on ice. The homogenate was centrifuged at 15,000 × g for 30 minutes and supernatant was used for further analysis by BCA protein assay and Western blot.

Supplementary Material

Refer to Web version on PubMed Central for supplementary material.

ACKNOWLEDGMENT

JG-98 was provided by J. Gestwicki at UCSF. Tau5 antibody was a gift from N. Kanaan at Michigan State University (originally created by L. Binder at Northwestern University). PHF1 was a gift from P. Davies. We thank the Chemical Purification Analysis and Screening (CPAS) core facility for using the Agilent LC-MS QqQ 6460. Some images were created using BioRender.com.

Funding Sources

Research reported in this publication was supported by Merit Review Award I01 BX002947 and I01 BX004626 from the United States (U.S.) Department of Veterans Affairs Biomedical Laboratory Research and Development Service. The views expressed in this article are those of the authors and do not necessarily reflect the position, policy or views of the Department of Veterans Affairs or the United States Government. This work was also supported by the National Institutes of Health/National Institutes on Aging RF1 AG055088 and R01 NS073899, which is co-funded by the National Institute of Neurological Disorders and Stroke and the National Institute on Aging. The content is solely the responsibility of the authors and does not necessarily represent the official views of the National Institutes of Health. This work has been supported in part by the Chemical Purification Analysis and Screening Core Facility (CPAS).

ABBREVIATIONS

HSPA	Heat shock protein 70kDa family
Hsc70	heat shock cognate 70 kDa
Hsp70	Heat shock protein 70 kDa
tau	microtubule associated protein tau
AD	Alzheimer’s disease
FTD	frontotemporal dementia
i.p.	intraperitoneal
PiD	Pick’s disease
PSP	progressive supranuclear palsy

NBD	nucleotide-binding domain
LDH	lactate dehydrogenase
PAMPA	parallel artificial membrane permeability assay
BBB	blood-brain barrier
ThT	Thioflavin
TEM	transmission electron microscopy

REFERENCES

(1). Feany MB; Dickson DW Neurodegenerative disorders with extensive tau pathology: a comparative study and review. Ann. Neurol 1996, 40 (2), 139–148. DOI: 10.1002/ana.410400204 [PubMed: 8773594]

(2). Kovacs GG Invited review: Neuropathology of tauopathies: principles and practice. Neuropathol. Appl. Neurobiol 2015, 41 (1), 3–23. DOI: 10.1111/nan.12208 [PubMed: 25495175]

(3). Tacik P; Sanchez-Contreras M; Rademakers R; Dickson DW; Wszolek ZK Genetic Disorders with Tau Pathology: A Review of the Literature and Report of Two Patients with Tauopathy and Positive Family Histories. NDD 2016, 16 (1–2), 12–21. DOI: 10.1159/000440840

(4). Irwin DJ Tauopathies as Clinicopathological Entities. Parkinsonism Relat. Disord 2016, 22 (0 1), S29–S33. DOI: 10.1016/j.parkreldis.2015.09.020 [PubMed: 26382841]

(5). Kovacs GG Tauopathies. Handb. Clin. Neurol 2017, 145, 355–368. DOI: 10.1016/B978-0-12-802395-2.00025-0 [PubMed: 28987182]

(6). Ghetti B; Oblak AL; Boeve BF; Johnson KA; Dickerson BC; Goedert M Invited review: Frontotemporal dementia caused by microtubule-associated protein tau gene (MAPT) mutations: a chameleon for neuropathology and neuroimaging. Neuropathol. Appl. Neurobiol 2015, 41 (1), 24–46. DOI: 10.1111/nan.12213 [PubMed: 25556536]

(7). Fischer D; Mukrasch MD; von Bergen M; Klos-Witkowska A; Biernat J; Griesinger C; Mandelkow E; Zweckstetter M Structural and microtubule binding properties of tau mutants of frontotemporal dementias. Biochemistry 2007, 46 (10), 2574–2582. DOI: 10.1021/bi061318s [PubMed: 17297915]

(8). Scholz T; Mandelkow E Transport and diffusion of Tau protein in neurons. Cell. Mol. Life Sci 2014, 71 (16), 3139–3150. DOI: 10.1007/s00018-014-1610-7 [PubMed: 24687422]

(9). Noble W; Hanger DP; Miller CC; Lovestone S The importance of tau phosphorylation for neurodegenerative diseases. Front. Neurol 2013, 4, 83. DOI: 10.3389/fneur.2013.00083 [PubMed: 23847585]

(10). Chang C-W; Shao E; Mucke L Tau: Enabler of diverse brain disorders and target of rapidly evolving therapeutic strategies. Science (New York, N.Y.) 2021, 371 (6532), eabb8255. DOI: 10.1126/science.abb8255

(11). Petrucelli L; Dickson D; Kehoe K; Taylor J; Snyder H; Grover A; De Lucia M; McGowan E; Lewis J; Prihar G; et al. CHIP and Hsp70 regulate tau ubiquitination, degradation and aggregation. Hum. Mol. Genet 2004, 13 (7), 703–714, Research Support, U.S. Gov't, P.H.S. DOI: 10.1093/hmg/ddh083 [PubMed: 14962978]

(12). Lu R-C; Tan M-S; Wang H; Xie A-M; Yu J-T; Tan L Heat Shock Protein 70 in Alzheimer's Disease. BioMed research international 2014, Review Article. (acccessed 2020/03/02/).

(13). Young ZT; Rauch JN; Assimon VA; Jinwal U; Ahn M; Li X; Dunyak BM; Ahmad A; Carlson G; Srinivasan SR; et al. Stabilizing the Hsp70-Tau Complex Promotes Turnover in Models of Tauopathy. Cell Chemical Biology 2016, 23 (8), 992–1001. DOI: 10.1016/j.chembiol.2016.04.014 [PubMed: 27499529]

(14). Kundel F; De S; Flagmeier P; Horrocks MH; Kjaergaard M; Shammas SL; Jackson SE; Dobson CM; Klenerman D Hsp70 Inhibits the Nucleation and Elongation of Tau and Sequesters

Tau Aggregates with High Affinity. ACS Chem. Biol 2018, 13 (3), 636–646. DOI: 10.1021/acschembio.7b01039 [PubMed: 29300447]

(15). Walter S; Buchner J Molecular chaperones--cellular machines for protein folding. Angew. Chem. Int. Ed. Engl 2002, 41 (7), 1098–1113. DOI: 10.1016/0959-440x(95)80014-r [PubMed: 12491239]

(16). Hervás R; Oroz J Mechanistic Insights into the Role of Molecular Chaperones in Protein Misfolding Diseases: From Molecular Recognition to Amyloid Disassembly. Int. J. Mol. Sci 2020, 21 (23), 9186. DOI: 10.3390/ijms21239186 [PubMed: 33276458]

(17). Radons J The human HSP70 family of chaperones: where do we stand? Cell Stress Chaperones 2016, 21 (3), 379–404. DOI: 10.1007/s12192-016-0676-6 [PubMed: 26865365]

(18). Drummond E; Pires G; MacMurray C; Askenazi M; Nayak S; Bourdon M; Safar J; Ueberheide B; Wisniewski T Phosphorylated tau interactome in the human Alzheimer's disease brain. Brain 2020, 143 (9), 2803–2817. DOI: 10.1093/brain/awaa223 [PubMed: 32812023]

(19). Tracy TE; Madero-Perez J; Swaney DL; Chang TS; Moritz M; Konrad C; Ward ME; Stevenson E; Huttenhain R; Kauwe G; et al. Tau interactome maps synaptic and mitochondrial processes associated with neurodegeneration. Cell 2022, 185 (4), 712–728 e714. DOI: 10.1016/j.cell.2021.12.041 [PubMed: 35063084]

(20). Abisambra JF; Jinwal UK; Blair LJ; O'Leary JC 3rd; Li Q; Brady S; Wang L; Guidi CE; Zhang B; Nordhues BA; et al. Tau accumulation activates the unfolded protein response by impairing endoplasmic reticulum-associated degradation. J. Neurosci 2013, 33 (22), 9498–9507. DOI: 10.1523/JNEUROSCI.5397-12.2013 [PubMed: 23719816]

(21). Fontaine SN; Rauch JN; Nordhues BA; Assimon VA; Stothert AR; Jinwal UK; Sabbagh JJ; Chang L; Stevens SM Jr.; Zuiderweg ER; et al. Isoform-selective Genetic Inhibition of Constitutive Cytosolic Hsp70 Activity Promotes Client Tau Degradation Using an Altered Co-chaperone Complement. J. Biol. Chem 2015, 290 (21), 13115–13127. DOI: 10.1074/jbc.M115.637595 [PubMed: 25864199]

(22). Fontaine SN; Martin MD; Akoury E; Assimon VA; Borysov S; Nordhues BA; Sabbagh JJ; Cockman M; Gestwicki JE; Zweckstetter M; et al. The active Hsc70/tau complex can be exploited to enhance tau turnover without damaging microtubule dynamics. Hum. Mol. Genet 2015, 24 (14), 3971–3981. DOI: 10.1093/hmg/ddv135 [PubMed: 25882706]

(23). Powers MV; Jones K; Barillari C; Westwood I; Montfort RLM; Workman P Targeting HSP70: The second potentially druggable heat shock protein and molecular chaperone? Cell Cycle 2010, 9 (8), 1542–1550. DOI: 10.4161/cc.9.8.11204 [PubMed: 20372081]

(24). Rousaki A; Miyata Y; Jinwal UK; Dickey CA; Gestwicki JE; Zuiderweg ER Allosteric Drugs: The Interaction of Antitumor Compound MKT-077 with Human Hsp70 Chaperones. J. Mol. Biol 2011, 411 (3), 614–632. DOI: 10.1016/j.jmb.2011.06.003 [PubMed: 21708173]

(25). Prince T; Ackerman A; Cavanaugh A; Schreiter B; Juengst B; Andolino C; Danella J; Chernin M; Williams H Dual targeting of HSP70 does not induce the heat shock response and synergistically reduces cell viability in muscle invasive bladder cancer. Oncotarget 2018, 9 (66), 32702–32717. DOI: 10.18632/oncotarget.26021 [PubMed: 30220976]

(26). Jinwal UK; Miyata Y; Koren J 3rd; Jones JR; Trotter JH; Chang L; O'Leary J; Morgan D; Lee DC; Shults CL; et al. Chemical manipulation of hsp70 ATPase activity regulates tau stability. J. Neurosci 2009, 29 (39), 12079–12088. DOI: 10.1523/JNEUROSCI.3345-09.2009 [PubMed: 19793966]

(27). Assimon VA; Gillies AT; Rauch JN; Gestwicki JE Hsp70 protein complexes as drug targets. Curr. Pharm. Des 2013, 19 (3), 404–417. DOI: 10.2174/138161213804143699 [PubMed: 22920901]

(28). Martin MD; Baker JD; Suntharalingam A; Nordhues BA; Shelton LB; Zheng D; Sabbagh JJ; Haystead TA; Gestwicki JE; Dickey CA Inhibition of Both Hsp70 Activity and Tau Aggregation in Vitro Best Predicts Tau Lowering Activity of Small Molecules. ACS Chem. Biol 2016, 11 (7), 2041–2048. DOI: 10.1021/acschembio.6b00223 [PubMed: 27177119]

(29). Shao H; Gestwicki JE Neutral analogs of the heat shock protein 70 (Hsp70) inhibitor, JG-98. Bioorg. Med. Chem. Lett 2020, 30 (5), 126954. DOI: 10.1016/j.bmcl.2020.126954 [PubMed: 31952963]

(30). Koren J 3rd; Miyata Y; Kiray J; O'Leary JC 3rd; Nguyen L; Guo J; Blair LJ; Li X; Jinwal UK; Cheng JQ; et al. Rhodacyanine derivative selectively targets cancer cells and overcomes tamoxifen resistance. PLoS One 2012, 7 (4), e35566. DOI: 10.1371/journal.pone.0035566 [PubMed: 22563386]

(31). Abisambra J; Jinwal UK; Miyata Y; Rogers J; Blair L; Li X; Seguin SP; Wang L; Jin Y; Bacon J; et al. Allosteric heat shock protein 70 inhibitors rapidly rescue synaptic plasticity deficits by reducing aberrant tau. Biol. Psychiatry 2013, 74 (5), 367–374. DOI: 10.1016/j.biopsych.2013.02.027 [PubMed: 23607970]

(32). Miyata Y; Li X; Lee H-F; Jinwal UK; Srinivasan SR; Seguin SP; Young ZT; Brodsky JL; Dickey CA; Sun D; et al. Synthesis and initial evaluation of YM-08, a blood-brain barrier permeable derivative of the heat shock protein 70 (Hsp70) inhibitor MKT-077, which reduces tau levels. ACS Chem. Neurosci 2013, 4 (6), 930–939. DOI: 10.1021/cn300210g [PubMed: 23472668]

(33). Li X; Srinivasan SR; Connarn J; Ahmad A; Young ZT; Kabza AM; Zuiderweg ER; Sun D; Gestwicki JE Analogs of the Allosteric Heat Shock Protein 70 (Hsp70) Inhibitor, MKT-077, as Anti-Cancer Agents. ACS Med. Chem. Lett 2013, 4 (11), 1042–1047. DOI: 10.1021/ml400204n [PubMed: 24312699]

(34). Yaglom JA; Wang Y; Li A; Li Z; Monti S; Alexandrov I; Lu X; Sherman MY Cancer cell responses to Hsp70 inhibitor JG-98: Comparison with Hsp90 inhibitors and finding synergistic drug combinations. Sci. Rep 2018, 8 (1), 1–12. DOI: 10.1038/s41598-017-14900-0 [PubMed: 29311619]

(35). Shao H; Li X; Hayashi S; Bertron JL; Schwarz DMC; Tang BC; Gestwicki JE Inhibitors of heat shock protein 70 (Hsp70) with enhanced metabolic stability reduce tau levels. Bioorg. Med. Chem. Lett 2021, 41, 128025. DOI: 10.1016/j.bmcl.2021.128025 [PubMed: 33839251]

(36). Shao H; Li X; Moses MA; Gilbert LA; Kalyanaraman C; Young ZT; Chernova M; Journey SN; Weissman JS; Hann B; et al. Exploration of Benzothiazole Rhodacyanines as Allosteric Inhibitors of Protein-Protein Interactions with Heat Shock Protein 70 (Hsp70). J. Med. Chem 2018, 61 (14), 6163–6177. DOI: 10.1021/acs.jmedchem.8b00583 [PubMed: 29953808]

(37). Li X; Colvin T; Rauch JN; Acosta-Alvear D; Kampmann M; Dunyak B; Hann B; Aftab BT; Murnane M; Cho M; et al. Validation of the Hsp70-Bag3 protein-protein interaction as a potential therapeutic target in cancer. Mol. Cancer Ther 2015, 14 (3), 642–648. DOI: 10.1158/1535-7163.MCT-14-0650 [PubMed: 25564440]

(38). Taylor IR; Assimon VA; Kuo SY; Rinaldi S; Li X; Young ZT; Morra G; Green K; Nguyen D; Shao H; et al. Tryptophan scanning mutagenesis as a way to mimic the compound-bound state and probe the selectivity of allosteric inhibitors in cells. Chem. Sci 2020, 11 (7), 1892–1904. DOI: 10.1039/c9sc04284a [PubMed: 34123282]

(39). Chang L; Bertelsen EB; Wisen S; Larsen EM; Zuiderweg ER; Gestwicki JE High-throughput screen for small molecules that modulate the ATPase activity of the molecular chaperone DnaK. Anal. Biochem 2008, 372 (2), 167–176. DOI: 10.1016/j.ab.2007.08.020 [PubMed: 17904512]

(40). Berben P; Bauer-Brandl A; Brandl M; Faller B; Flaten GE; Jacobsen AC; Brouwers J; Augustijns P Drug permeability profiling using cell-free permeation tools: Overview and applications. Eur. J. Pharm. Sci 2018, 119, 219–233. DOI: 10.1016/j.ejps.2018.04.016 [PubMed: 29660464]

(41). Radan M; Djikic T; Obradovic D; Nikolic K Application of in vitro PAMPA technique and in silico computational methods for blood-brain barrier permeability prediction of novel CNS drug candidates. Eur. J. Pharm. Sci 2022, 168, 106056. DOI: 10.1016/j.ejps.2021.106056 [PubMed: 34740787]

(42). Baker JD; Shelton LB; Zheng D; Favretto F; Nordhues BA; Darling A; Sullivan LE; Sun Z; Solanki PK; Martin MD; et al. Human cyclophilin 40 unravels neurotoxic amyloids. PLoS Biol. 2017, 15 (6), e2001336. DOI: 10.1371/journal.pbio.2001336 [PubMed: 28654636]

(43). Shelton LB; Baker JD; Zheng D; Sullivan LE; Solanki PK; Webster JM; Sun Z; Sabbagh JJ; Nordhues BA; Koren J 3rd; et al. Hsp90 activator Aha1 drives production of pathological tau aggregates. Proc. Natl. Acad. Sci. U. S. A 2017, 114 (36), 9707–9712. DOI: 10.1073/pnas.1707039114 [PubMed: 28827321]

(44). Santacruz K; Lewis J; Spires T; Paulson J; Kotilinek L; Ingelsson M; Guimaraes A; DeTure M; Ramsden M; McGowan E; et al. Tau suppression in a neurodegenerative mouse model

improves memory function. Science (New York, N.Y.) 2005, 309 (5733), 476–481. DOI: 10.1126/science.1113694 (acccessed Jul 15). [PubMed: 16020737]

(45). Dickey C; Kraft C; Jinwal U; Koren J; Johnson A; Anderson L; Lebson L; Lee D; Dickson D; de Silva R; et al. Aging analysis reveals slowed tau turnover and enhanced stress response in a mouse model of tauopathy. Am. J. Pathol 2009, 174 (1), 228–238. DOI: 10.2353/ajpath.2009.080764 [PubMed: 19074615]

(46). Soeda Y; Saito M; Maeda S; Ishida K; Nakamura A; Kojima S; Takashima A Methylene Blue Inhibits Formation of Tau Fibrils but not of Granular Tau Oligomers: A Plausible Key to Understanding Failure of a Clinical Trial for Alzheimer's Disease. Journal of Alzheimer's disease: JAD 2019, 68 (4), 1677–1686. DOI: 10.3233/JAD-181001 [PubMed: 30909223]

(47). Lo Cascio F; Kayed R Azure C Targets and Modulates Toxic Tau Oligomers. ACS Chem. Neurosci 2018, 9 (6), 1317–1326. DOI: 10.1021/acschemneuro.7b00501 [PubMed: 29378132]

(48). Miyata Y; Rauch JN; Jinwal UK; Thompson AD; Srinivasan S; Dickey CA; Gestwicki JE Cysteine reactivity distinguishes redox sensing by the heat-inducible and constitutive forms of heat shock protein 70. Chem. Biol 2012, 19 (11), 1391–1399. DOI: 10.1016/j.chembiol.2012.07.026 [PubMed: 23177194]

(49). Crowe A; James MJ; Lee VMY; Smith AB; Trojanowski JQ; Ballatore C; Brunden KR Aminothienopyridazines and Methylene Blue Affect Tau Fibrillization via Cysteine Oxidation. The Journal of biological chemistry 2013, 288 (16), 11024–11037. DOI: 10.1074/jbc.M112.436006 [PubMed: 23443659]

(50). Taniguchi S; Suzuki N; Masuda M; Hisanaga S-i.; Iwatsubo, T.; Goedert, M.; Hasegawa, M. Inhibition of Heparin-induced Tau Filament Formation by Phenothiazines, Polyphenols, and Porphyrins. J. Biol. Chem 2005, 280 (9), 7614–7623. DOI: 10.1074/jbc.M408714200 [PubMed: 15611092]

(51). Meng F; Marek P; Potter KJ; Verchere CB; Raleigh DP Rifampicin does not prevent amyloid fibril formation by human islet amyloid polypeptide but does inhibit fibril thioflavin-T interactions: implications for mechanistic studies of beta-cell death. Biochemistry 2008, 47 (22), 6016–6024. DOI: 10.1021/bi702518m [PubMed: 18457428]

(52). Kroes-Nijboer A; Lubbersen YS; Venema P; Linden E Thioflavin T fluorescence assay for β-lactoglobulin fibrils hindered by DAPH. J. Struct. Biol 2009, 165 (3), 140–145. DOI: 10.1016/j.jsb.2008.11.003 [PubMed: 19063973]

(53). Hudson SA; Ecroyd H; Kee TW; Carver JA The thioflavin T fluorescence assay for amyloid fibril detection can be biased by the presence of exogenous compounds. The FEBS Journal 2009, 276 (20), 5960–5972. DOI: 10.1111/j.1742-4658.2009.07307.x [PubMed: 19754881]

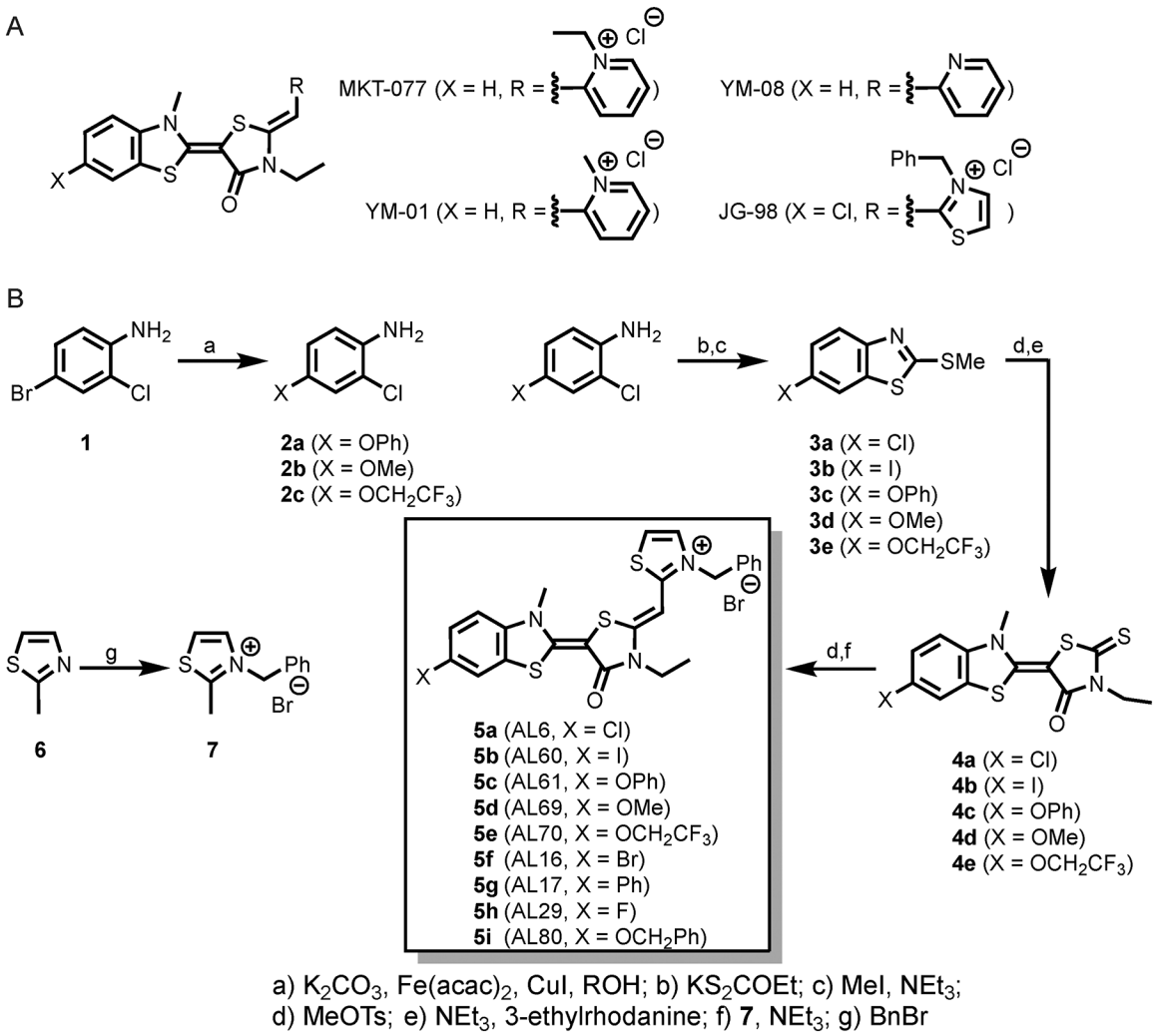

Figure 1: Synthesis of rhodacyanine compounds.

A: Primary HSPA rhodacyanine compounds. **B**: Scheme for the synthesis of the HSPA rhodacyanine analogs AL6, AL60, AL61, AL69, AL70, AL16, AL17, AL29, and AL80 used in this study.

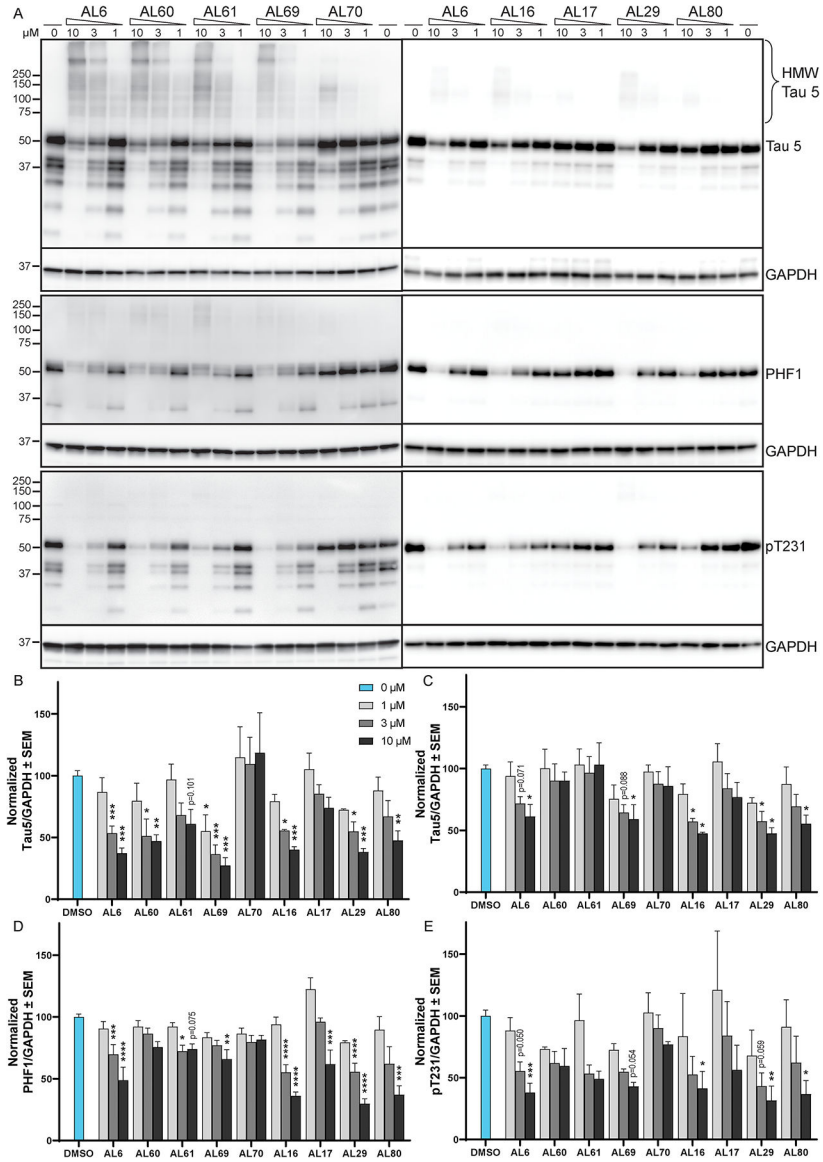

Figure 2: Select benzothiazole-substituted rhodacyanine compounds potently reduce tau levels in iHekP301L cells.

A: Representative Western blots of lysates from inducible tau P301L (iHekP301L) cells incubated with the indicated compounds or a DMSO vehicle are shown. Tau5 antibody detects total tau protein, PHF1 antibody detects tau phosphorylated at S396 and S404, and pT231 detects tau phosphorylated at T231. Antibodies used for left and right blots are shown on the right. Quantitation of signal near the ~50 kda band of **B**: Tau5 and total signal in the full lane of **C**: Tau5, **D**: PHF1 (pS396/S404 tau), **E**: pT231 tau normalized to GAPDH. Statistical analysis of the mean ± SEM from 3 independent experiments was evaluated by one-way ANOVA using Dunnett's post-hoc comparison to the DMSO vehicle control condition (* $p<0.05$; ** $p<0.01$; *** $p<0.001$).

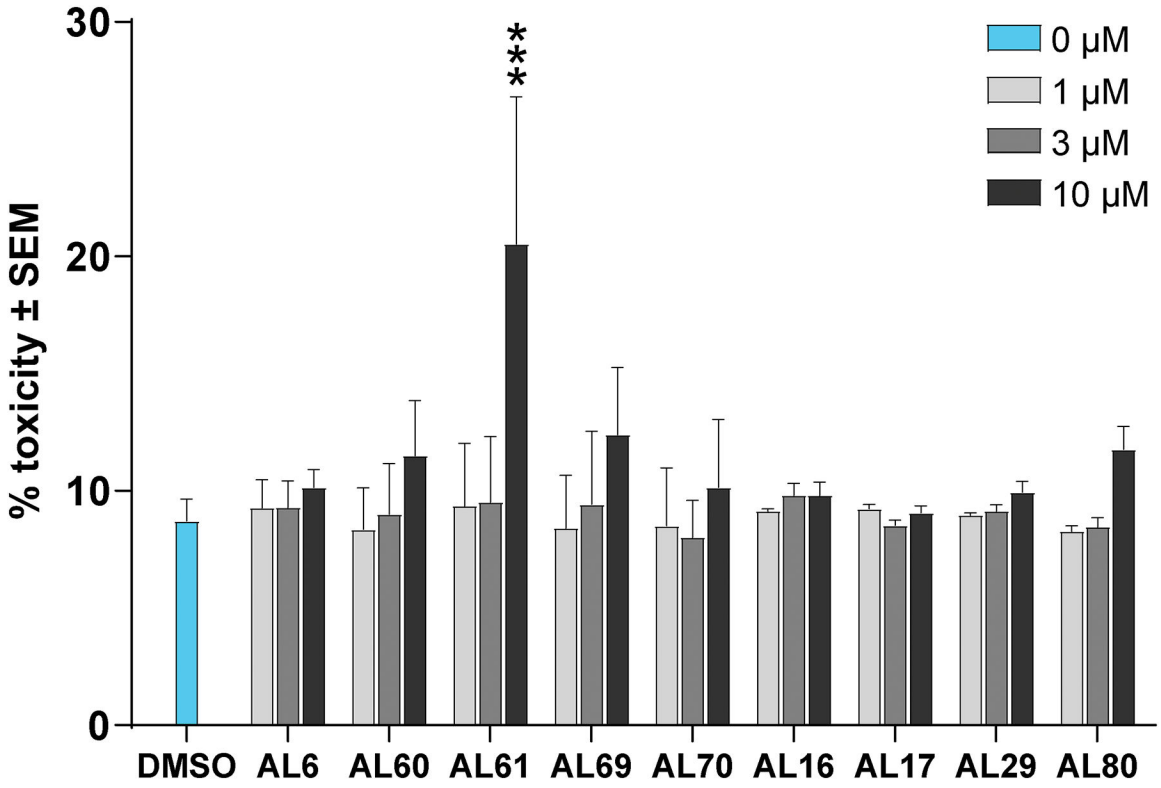

Figure 3: Most rhodacyanine analogs show no cellular toxicity.

Toxicity after 24-hour treatment of each compound in cultured SH-SY5Y human neuroblastoma cells was measured using an LDH assay. Values are expressed in % toxicity, which is the mean percent of extracellular LDH measured, relative to a control sample of completely lysed cells, from three independent experiments (± SEM). Statistical analysis was evaluated by one-way ANOVA using Dunnett's post-hoc multiple comparisons test (*** $p<0.001$) to the DMSO control.

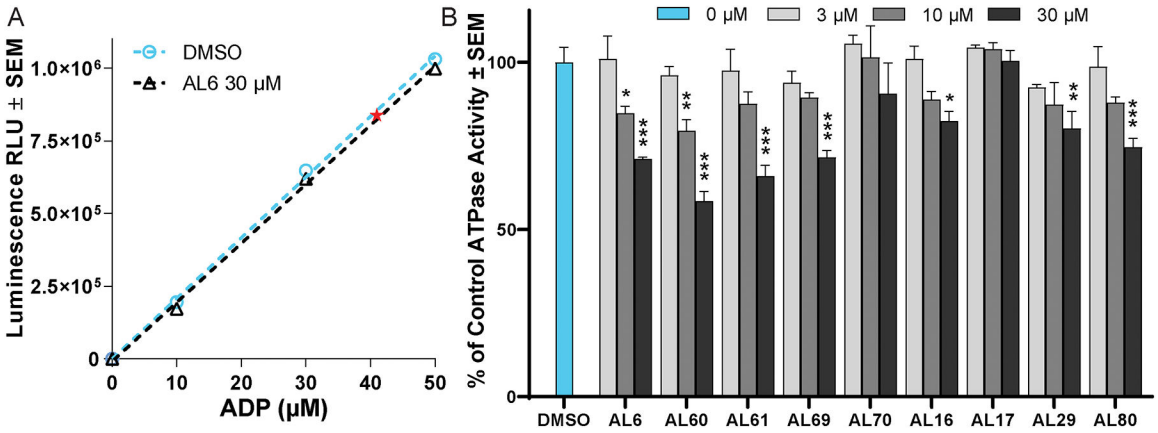

Figure 4: Rhodacyanine compounds inhibit recombinant Hsc70 ATPase activity.

A: ADP standard curve in the presence of 1% DMSO (vehicle control) compared to AL6 at 30 μM. Linear regression analysis confirmed the slopes and y-intercepts were not statistically different. The red star indicates the luminescence signal measured for Hsc70 ATPase activity in the presence of 1% DMSO. **B**: Percentage of ATPase activity relative to 1% DMSO (vehicle control). Data shown are the mean ± SEM from one representative experiment performed in triplicate. Statistical analysis of each compound relative to the DMSO control was evaluated by one-way ANOVA using Dunnett's post-hoc multiple comparison test (* $p<0.05$. ** $p<0.01$, *** $p<0.001$).

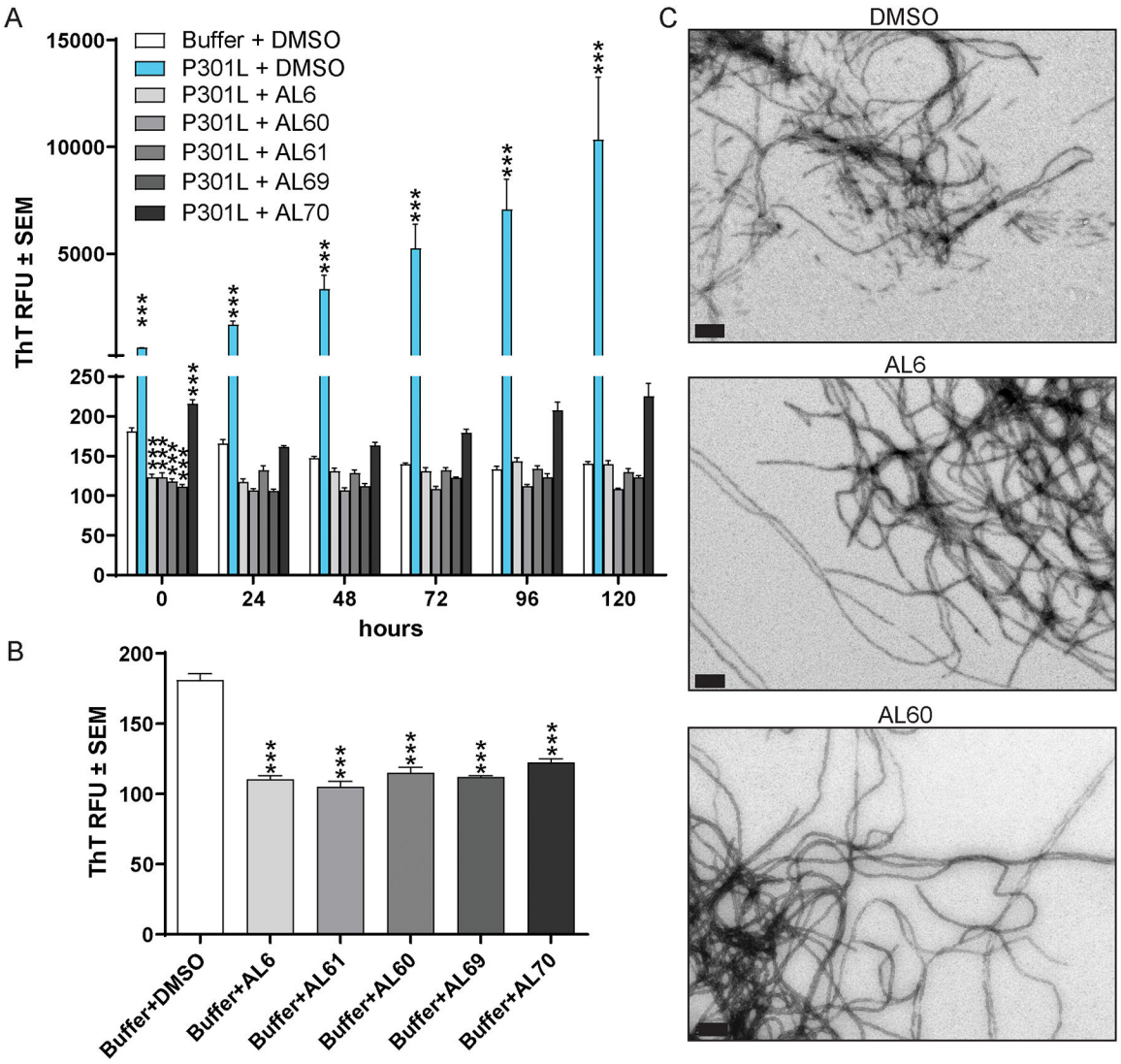

Figure 5: Rhodacyanine analogs are not compatible with the ThT tau aggregation assay and do not directly inhibit heparin-induced tau aggregation.

A: Thioflavin T (ThT) fluorescence signal in relative fluorescent units (RFUs) over 5 days of incubation with heparin and tau P301L protein in the presence of DMSO vehicle or the indicated compounds at 10 μM. Data shown are the means of 6 replicates for each condition (± SEM). Statistical analysis was evaluated by one-way ANOVA using Dunnett's post-hoc comparison to the Buffer + DMSO vehicle control condition at each timepoint (*** $p<0.001$). **B**: Initial ThT at T=0 hours at 10 μM compound compared to DMSO control. Data shown are the means of 2–4 replicates for each condition (± SEM). Statistical analysis was evaluated by one-way ANOVA using Dunnett's post-hoc comparison to the Buffer + DMSO vehicle control condition (*** $p<0.001$). **C**: Representative 60,000× TEM images of aggregated tau protein from day 5 of the *in vitro* aggregation assay in the presence of DMSO vehicle, AL6, or AL60. Scale bars = 200 nm.

A

	PAMPA membrane permeability (%)	Retained in PAMPA membrane (%)	clogP
AL6	0	59	2.96
AL60	0	60	3.37
AL61	0	71	4.16
AL69	0	31	2.09
AL70	0	44	2.89
AL16	0	42	3.11
AL17	0	81	3.95
AL29	0	32	2.39
AL80	0	95	3.86

B

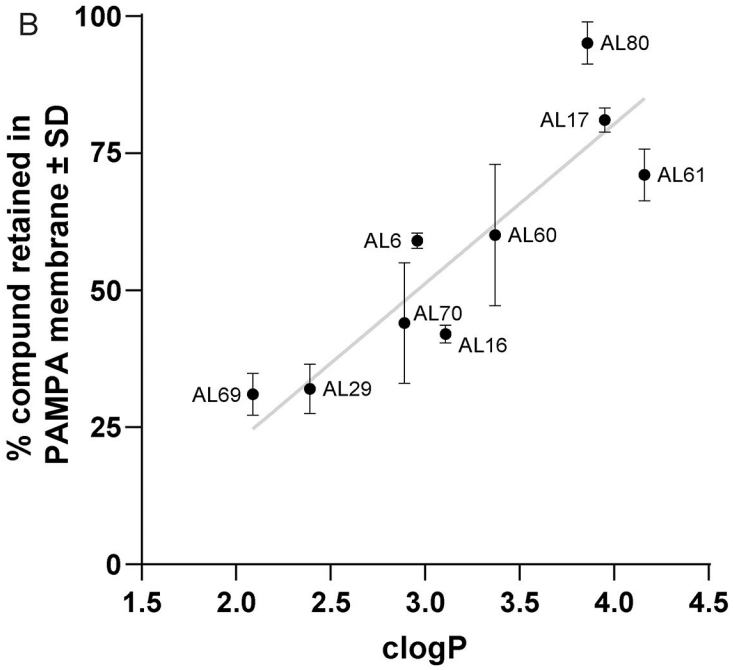

Figure 6: PAMPA membrane data and correlation of clogP to BBB-PAMPA membrane retention.

A: PAMPA membrane permeability, retention, and calculated clogP for rhodacyanine analogs. **B**: A graph of the clogP and BBB-PAMPA membrane retention. A simple linear regression fit line is shown in grey.

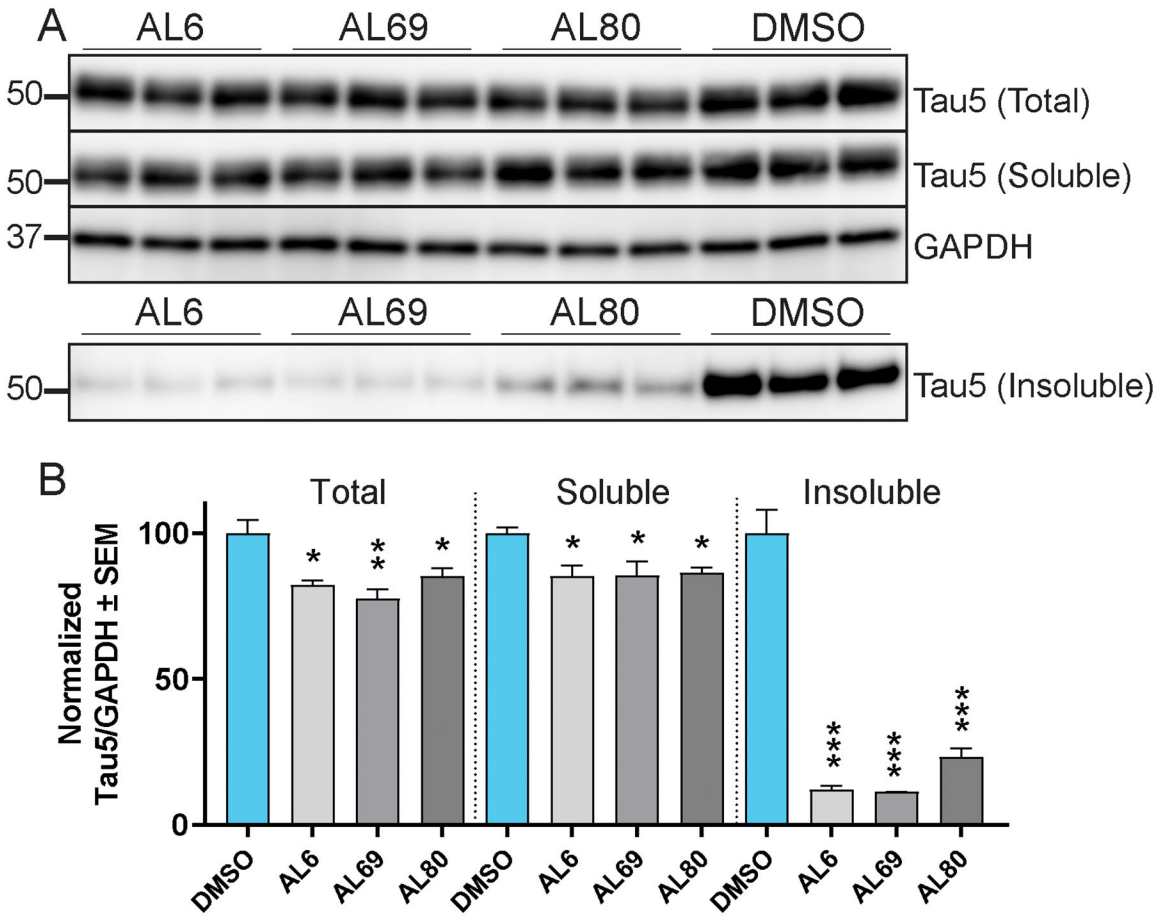

Figure 7: Rhodacyanine analogs, AL6, AL69, and AL80 reduce total, soluble, and insoluble tau levels in iHekP301L cells.

A: Representative Western blots of fractionated lysates into total, soluble, and insoluble tau from inducible tau P301L (iHekP301L) cells incubated with AL6, AL69, AL80, or DMSO vehicle are shown. Tau5 antibody detects total tau protein. **B**: Quantitation of total tau prior to fractionation, soluble tau, and insoluble tau normalized to GAPDH. For insoluble tau, GAPDH from the soluble blot was used for normalization. Statistical analysis of the mean ± SEM from 3 replicates was evaluated by one-way ANOVA using Dunnett's post-hoc comparison to the DMSO vehicle control condition (* $p<0.05$; ** $p<0.01$; *** $p<0.001$).

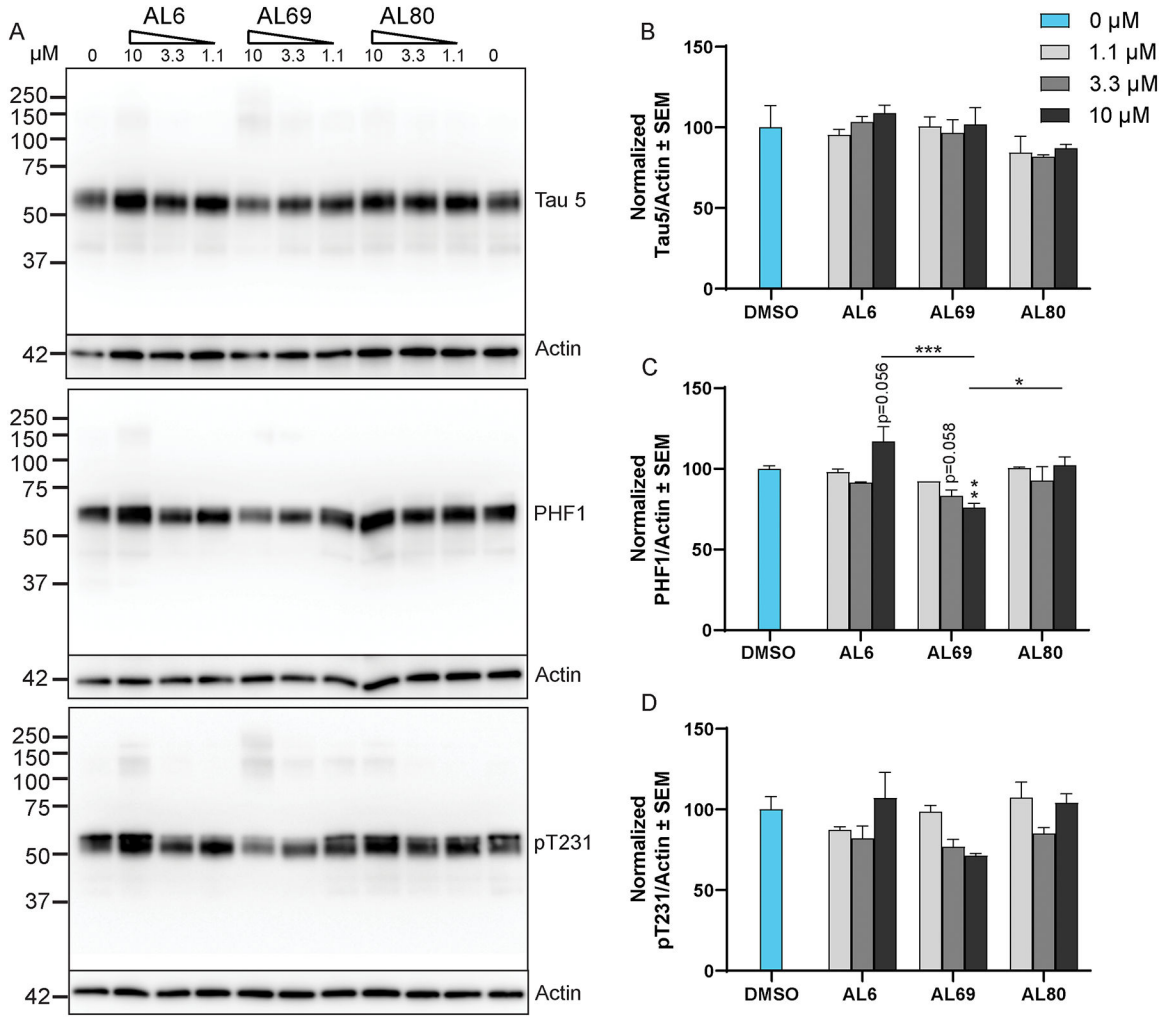

Figure 8: Rhodacyanine compounds modulate the levels of phosphorylated tau in *ex vivo* brain slices from rTg4510 mice.

A: Representative Western blots of *ex vivo* brain slices from N=3 mice treated with DMSO control, AL6, AL69, or AL80, as indicated. Quantitation of total signal in the full lane of **B**: Tau5, **C**: PHF1 (pS396/S404 tau), **D**: pT231 tau normalized to Actin. Statistical analysis of the mean ± SEM, from 2 technical Western blot replicates were evaluated by one-way ANOVA using Dunnett's post-hoc comparison to the DMSO vehicle control condition (*p<0.05; **p<0.01; ***p<0.001).